Journal of Non-Crystalline Solids 358 (2012) 2559–2570

Contents lists available at SciVerse ScienceDirect

Journal of Non-Crystalline Solids

journal homepage: www.elsevier.com/ locate/ jnoncrysol

Effect of composition on the short-term and long-term dissolution rates of ten borosilicate glasses of increasing complexity from 3 to 30 oxides

Stéphane Gin *, Xavier Beaudoux, Frédéric Angéli, Christophe Jégou, Nicole Godon

CEA, DEN–Marcoule, F-30207 Bagnols-sur-Cèze, France

ARTICLE INFO

Article history:
Received 2 February 2012
Received in revised form 5 April 2012
Available online 7 July 2012

Keywords:
Glass;
Dissolution;
Rate;
Residual rate;
Composition

ABSTRACT

Ten borosilicate glass compositions consisting of a ternary sodium borosilicate containing increasing numbers of some of the key elements (Al, Ca, Zr, Ce) present in nuclear glasses were leached in pure water at 90 °C and monitored for up to 14 years. They were then characterized to establish correlations between the glass composition and the short- and long-term alteration rates. We first qualitatively explain the variations of the initial dissolution rate by structural considerations. Then we evidence a qualitative inverse correlation between the initial and residual rates. This counterintuitive result is in fact related to the effect of gel reorganization on the diffusive properties of the passivating layer. Since no equilibrium can be reached between glass and solution, these long-term experiments help in understanding how glasses behave once the solution is saturated with respect to the main glass formers. Very efficient synergy between Ca and hardener elements (Al or Zr) leads to the lowest residual rates, compared with glasses having only one of the two categories of elements. We also confirm the detrimental effect of precipitation of silicate minerals on the residual rate.

1. Introduction

In France, spent nuclear fuel is reprocessed and the remaining high-level waste is vitrified. The resulting borosilicate glass, generally composed of around 30 different oxides, will probably be stored eventually in a deep geological formation. Leaching by groundwater is known to be the main phenomenon by which radionuclides could be released from the glass and migrate through the host rock. It is thus of primary importance to elucidate the mechanisms controlling the long-term dissolution rate and the effects of intrinsic and environmental parameters on these mechanisms [1]. This is one of the perquisites for demonstrating the safety of a geological repository. Here, following a parametric approach, we focus on the effect of some of the main glass components on the different kinetic regimes, with emphasis on the long-term rate, also called the residual rate, because it is the main kinetic regime expected in a geological repository and, as previously shown, large composition variations are expected within the actual glass [2,3].

Previous studies have shown that it is possible to investigate the effect of glass composition by working on simple materials [4–7]. The advantage is that potential couplings and nonlinear effects can be evidenced progressively. Here we have chosen to apply this methodology by focusing on nine simplified glass compositions derived from SON68 glass, which is the inactive surrogate of the French reference glass for high-level waste arising from PWR fuel. Based on results of leach tests exceeding 10 years and post-mortem characterization by scanning electron microscopy (SEM), transmission electron microscopy (TEM) and X-ray diffraction (XRD), this paper establishes relations between the glass compositions, the properties of the alteration layer, and the dissolution kinetics.

2. Methodology

Nine simplified glasses (CJ1 to CJ9) and one complex glass (SON68) were fabricated and studied. The simple glass series was built by adding new oxides one by one to the (SiO_2, B_2O_3, Na_2O) ternary system. The elemental molar ratios of all the simple glasses except CJ6 were identical with those of the major elements of SON68 glass. The Ce present in CJ6 glass simulates all the rare earth elements of SON68 glass (La, Ce, Pr, Nd); in order to incorporate this amount of Ce it was necessary to add more alkali, so we decided to add Li in the same amount as in SON68 glass. According to the strategy adopted to formulate this set of glasses, none of them has the same set of oxides in their composition. By comparing one glass to another, this approach allows us to qualitatively assess the effect of each element, and thus to dissociate the role of Al, Ca, Zr and Ce on the glass durability. Some glasses were designed to study the effect of a single element (Al in CJ2 and Ca in CJ8, by comparison with CJ1), and others to reveal interactions between them. More particularly, we investigated the role of the interactions between Al and Ca (CJ3, CJ4) and between Zr and Ca (CJ4, CJ9). Long-term experiments consisted in analyzing the elements released into solution during 11 to 14 years (depending

* Corresponding author.
E-mail address: stephane.gin@cea.fr (S. Gin).

0022-3093/$ – see front matter © 2012 Elsevier B.V. All rights reserved.
doi:10.1016/j.jnoncrysol.2012.05.024

on the tests) and the glass alteration products at the end of the test by SEM, TEM and XRD.

3. Experimental

3.1. Glass composition

The theoretical composition of the 10 studied glasses (oxide wt.%) and some of their properties are indicated in Table 1.

The compositions of these glasses were checked by Inductively Coupled Plasma-Atomic Emission Spectroscopy (ICP-AES) after caustic fusion ($NaOH–KNO_3$ and lithium tetraborate) of glass powders. The experimental results being very close to the expected ones (differences were below the experimental uncertainties, which are typically 3% for the major elements and 5% for the other), the values in Table 1 were used for the calculations. The glasses were heated to T_m (see Table 1) for 3 h in a platinum crucible, according to the method described by Pacaud et al. and annealed for 1 h between 530 °C and 590 °C in a graphite crucible [8]. The homogeneity of glasses CJ1 to CJ6 was checked by Rayleigh–Brillouin light scattering and leads to Landau–Placzek ratios ranging from 50 to 200, indicating that these glasses contained no heterogeneities exceeding 15 Å[9]. The microscopic homogeneity of the other glasses was checked by optical and SEM observations. The density of each glass was determined with a hydrostatic balance and ranged from 2.40 to 2.75 $g\cdot cm^{-3}$.

3.2. Leaching experiments

The initial dissolution rate of the 10 glasses was determined by static leaching experiments in pure water with the 100–125 μm powder fraction buffered at pH 9 (0.1N KOH) at 90 °C (±1 °C), with a glass-surface-area-to-solution-volume (*SA/V*) ratio of 10 m^{-1}. The specific surface area of the glass powder was measured by krypton adsorption using the BET method. The range of values for this size fraction is between 0.04 and 0.058 $m^2\cdot g^{-1}$; the SA/V was then adjusted by measurement of the solution volume. The test vessel was a 1-liter PTFE reactor in which the solution was continuously homogenized by a magnetic stirring rod. Solution samples were taken at regular intervals, acidified with 1N HNO_3 and analyzed by ICP-AES. Although a flow-through protocol is generally preferable to accurately measure the initial dissolution rate, as the concentrations in solution are maintained constant at a low level during the measurement, we took care to keep the solution sufficiently diluted and measured the initial dissolution rate when glass dissolution was congruent and when the release of the main glass components (Si, B, Na) was linear.

Long-term static tests were performed at 90 °C (±1 °C), in initially pure water, with a SA/V of 8000 m^{-1}, except for CJ9 for which the test was conducted with a SA/V of 17,000 m^{-1} due to the greater specific surface area of the glass powder, determined after the test began. This difference by a factor two can be expected to slightly shorten the duration of the rate drop regime for CJ9 glass compared with the other glasses, but has a negligible impact on the residual rate. This has been clearly evidenced on SON68 glass [10].

The glass powder used for these static tests ranged from 40 to 100 μm and the specific surface area of these materials ranged from 0.063 to 0.173 $m^2\cdot g^{-1}$. Details are given in the Supporting information. The test vessel was a PTFE reactor filled with 300 mL of deionized water and placed in a 1 L PTFE vessel itself containing few milliliters of deionized water to limit evaporation from the reactor containing the glass. The pH was checked regularly and solution samples of 1 mL each were taken at different intervals, then acidified and analyzed by ICP-AES. At the beginning of April 2011, a sample of a few grams of glass powder was taken for solid characterization (XRD, SEM and TEM). Because all the tests did not start at the same time, this sampling date corresponds to the following leaching durations: 13.6 years for CJ1, 14.4 years for CJ2 to CJ6, and 12.8 years for the others.

3.3. Solution analyses

Concentrations of Si, B and Na were determined by ICP-AES in each sample. In some cases the Al, Ca, Li or Zr concentrations were also analyzed. The detection limits were 50, 20, 20, 20, 100, 200 and 500 $\mu g\cdot L^{-1}$ for Si, B, Li, Zr, Al, Na, and Ca, respectively. The background concentrations in the starting solution were systematically below the detection limits. The uncertainties were 3% for Si, B, Na and Li and 5% for Al and Ca. Zr was systematically below the detection limit.

To calculate the equivalent thickness of altered glass from given element *i*, $ET(i)$, a spherical shrinking-core model was used to account for the reduction in surface area due to alteration. The following formulas were applied (see Chave et al. [11] for more details):

$$\%AG = 100\cdot\frac{V_0-V_t}{V_0} = 100\cdot\left(1-\frac{V_t}{V_0}\right) = 100\cdot\left(1-\frac{R_t^3}{R_0^3}\right) \quad (1)$$

$$R_0 = \frac{3}{\rho S_{BET}} \quad (2)$$

where $\%AG$ is the percentage of altered glass, *V* and *R* respectively the volume and radius of each grain (the subscript 0 refers to the initial state and *t* to the corresponding sampling time), ρ is the glass density ($g\cdot m^{-3}$) and S_{BET} the specific surface area measured by BET ($m^2\cdot g^{-1}$). R_0 is thus not determined from the particle size, but from the specific surface area. Eqs. (1) and (2) lead to:

$$ET(i) = R_0-R_i(t) = R_0\left(1-\frac{R_i(t)}{R_0}\right) = \frac{3}{\rho S_{BET}}\left(1-\left(\frac{100-\%AG}{100}\right)^{1/3}\right). \quad (3)$$

The altered glass percentage at time t_n, $\%AG(t_n)$,is calculated from the mass balance between two samples, with allowance for the leaching solution volume variation due to the analysis samples:

$$\%AG(t_n) = \frac{{}^{C_i(t_n)V(t_n)}\big/_{M_i}}{mX_i} + \%AG(t_{n-1}) \quad (4)$$

Table 1
Properties of the 10 studied glasses: theoretical composition (wt%), melting temperature (T_m), density (ρ).

Glass	Index	SiO_2	B_2O_3	Na_2O	Li_2O	Al_2O_3	CaO	ZrO_2	Ce_2O_3	Other	T_m (°C)	ρ ($g\cdot cm^{-3}$)
T	CJ 1	65.6	20.2	14.2	–	–	–	–	–	–	1500	2.45
T + Al	CJ 2	61.2	18.9	13.3	–	6.6	–	–	–	–	1450	2.41
T + Al + Ca	CJ 3	58.1	17.9	12.6	–	6.3	5.1	–	–	–	1400	2.47
T + Al + Ca + Zr	CJ 4	56.2	17.3	12.2	–	6.0	5.0	3.3	–	–	1400	2.50
T + Al + Ca + Zr + Ce	CJ 5	55.6	17.1	12.0	–	6.0	4.9	3.2	1.2	–	1400	2.52
T + Al + Ca + Zr + Ce + Li	CJ 6	52.3	16.2	11.3	2.3	5.7	4.6	3.1	4.5	–	1450	2.61
T + Al + Zr	CJ 7	59.1	18.2	12.8	–	6.4	–	3.5	–	–	1400	2.43
T + Ca	CJ 8	62.0	19.1	13.4	–	–	5.5	–	–	–	1400	2.51
T + Ca + Zr	CJ 9	59.8	18.4	13.0	–	–	5.3	3.5	–	–	1350	2.55
SON68	SON68	45.1	13.9	10.1	2.0	4.9	4.0	2.7	1.0	16.3	–	2.76

where $C_i(t_n)$ is the concentration ($g \cdot m^{-3}$) of element i in solution at time t_n, X_i the mass fraction of i in the glass, M_i its molar mass ($g \cdot .mol^{-1}$), V the solution volume (m^3), and m the powder mass. Due to solution and powder sampling, m and V were adjusted at each sampling interval.

The normalized mass loss of the glass calculated from element i, $NL(i)$ (in $g \cdot m^{-2}$), and the retention factor of element i in the alteration products, $RF(i)$, can be easily calculated:

$$NL(i) = ET(i) \times \rho_g \tag{5}$$

$$RF(i) = 1 - \frac{NL(i)}{NL(\mathrm{B})} \tag{6}$$

Boron is a good alteration tracer under our test conditions, as it is primarily a network former and is not retained in the alteration products [12].

The glass alteration rate ($g \cdot m^{-2}\, d^{-1}$) is then used to determine the initial and the residual alteration rates of the glasses (respectively r_0 and r_r):

$$r(i,t) = \frac{dNL(i,t)}{dt}. \tag{7}$$

During the initial alteration stage most of the elements are released linearly and congruently at the maximum rate (for given temperature and pH conditions) controlled by hydrolysis of the silicate network. The initial rate, which corresponds to this maximum dissolution rate, is simply deduced from the slope of the straight line $NL(\mathrm{B}) = f(t)$.

In general, the transition between the rate drop and the residual rate occurs once the solution is saturated with respect to silica. Here, the activity of silica was calculated by the JChess geochemical code [13] using the CTDP thermodynamic database [14]. Silica species taken into account are mainly H_4SiO_4, $H_3SiO_4^-$ ($H_2SiO_4^{2-}$ can be estimated but remains very low due to the pH) and $NaHSiO_3$. Note that, oligomers and other nanocolloids potentially present in the leachates have not been considered, neither experimentally, nor by calculation.

The activity of silica was no longer constant in our experiment. Consequently, it was decided to plot the activity of silica versus the glass dissolution rate. As a result, a clear turning point appeared. Before this point the rate decreases sharply as the activity of silica increases rapidly. Beyond this point both parameters still evolve, but very slowly. This turning point, and the corresponding time, t_r, was chosen to mark the transition between the two kinetic regimes.

In the residual rate regime, the glass dissolution rate is no longer driven by hydrolysis of the pristine glass but rather by a diffusion process [15–18]. The apparent diffusion coefficients of mobile species through the passivating part of the alteration layer, called the passivating reactive interphase (PRI), were calculated from Fick's second law. Here, the assumption of a semi-infinite medium leads to an increase in the PRI thickness with the square root of D as described in Eq. (8a):

$$e = 2\sqrt{\frac{Dt}{\Pi}} \tag{8a}$$

which gives

$$D = s^2 \times \frac{\Pi}{4} \tag{8b}$$

where s is the slope of the curve $e = f(t^{0.5})$, and $e = ET(\mathrm{B}) - ET(\mathrm{Si})$.

Uncertainties were calculated from the uncertainty propagation law. The relative uncertainties were ±6% for NL(Si, B, Na, Ca) and ET(B), ±10% for r_0 and ±20% for r_r.

3.4. SEM analyses

Morphological and chemical analyses were carried out on a JEOL 6330 Field Emission Scanning Electron Microscope equipped with an Energy-Dispersive Spectrometer system.

3.5. Focused ion beam milling

Ultrathin samples were prepared for TEM characterization. Focused ion beam (FIB) milling was performed with an FEI 200 TEM FIB system at the University of Aix-Marseille III. We used the same procedure as described by Benzerara et al. [19]. The same area as observed by SEM was located using FIB imaging capabilities. The FIB cross-section was prepared using a 30 kV Ga^+ beam operating at ~20 nA. The prepared cross-section measuring approx. 12 μm × 5 μm × 0.15 μm was transferred at atmospheric pressure with a micromanipulator to the membrane of a carbon-coated 200 mesh copper grid.

3.6. TEM and EDX analyses

TEM analyses were carried out on two microscopes. The morphological observations were made on a JEOL JEM 2010F microscope operating at 200 kV, equipped with a field emission gun, a high-resolution UHR pole piece and a Gatan GIF200 energy filter. Energy-dispersive X-ray (EDX) analyses were carried out on a Tecnai G2 (FEI), equipped with a LaB6 source operating at 200 kV. The detectors were a Gatan CCD 6 camera, a STEM BF-DF detector and an EDAX Genesis for the EDX analyses. The spatial resolution was 0.27 nm.

3.7. X-ray diffraction

The crystal structure on the altered glass surfaces was examined by XRD using a Philips X′Pert diffractometer equipped with a copper tube (1.54 Å) used at 40 kV and 40 mA in goniometer configuration in 0.017° steps at 2 s/step with a 1/4° forward anti-scatter slit and 1/2° forward divergence and back anti-scatter slits. The samples were altered powders after drying.

4. Results

4.1. Solution analyses

4.1.1. Initial dissolution rate

In this paper, we show and discuss leaching data covering up to 14.4 years (Table 2). Because the initial dissolution rate is generally not maintained for a long time (likely around half an hour in the test run at 8000 m^{-1}), specific experiments were performed in dilute conditions to measure this maximum dissolution rate of the ten glasses. Results and interpretation have been published in Ref. [9]. Congruent and linear release of Si, B and Na was observed for all the studied glasses up to around 3% of the Si concentration at saturation, which was finally reached after 1 year in the long-term experiment (apparent saturation). Further experiments under flow-through conditions confirmed the initial dissolution rate values given in Table 1 (unpublished data). Globally, for the set of tested glasses, the initial dissolution rates, r_0, are of the same order of magnitude (between ~1 and ~10 $g \cdot m^{-2} d^{-1}$). First, we may note that the r_0 value of the ternary glass CJ1 is only twice that of SON68 glass. The different components added to the CJ1 glass can weaken or harden the silicate network, so one-to-one glass comparisons may make it possible to reveal the role of each element. This approach is only qualitative, however, as in our series of glasses the addition of one element to the previous glass impacted the entire composition. Consequently, a modification of the initial rate can be due either to the added element, or to the diminishing amounts of the other elements, or both. In any event, it can be stated without ambiguity that the addition of Al to CJ1 (glass CJ2) significantly decreases r_0. Zr also works the same way, notably when comparing CJ3 and CJ4 (or CJ8 and CJ9), but the difference between CJ2 and CJ7 is not significant, perhaps because Al and Zr have a similar effect and Al is 4.5 times more abundant than Zr in these glasses. Conversely, the addition of Ca to CJ2 (glass CJ3), and to CJ1 (glass CJ8) leads to a significant increase in r_0. This can be due to a specific effect of Ca and/or a decrease in the

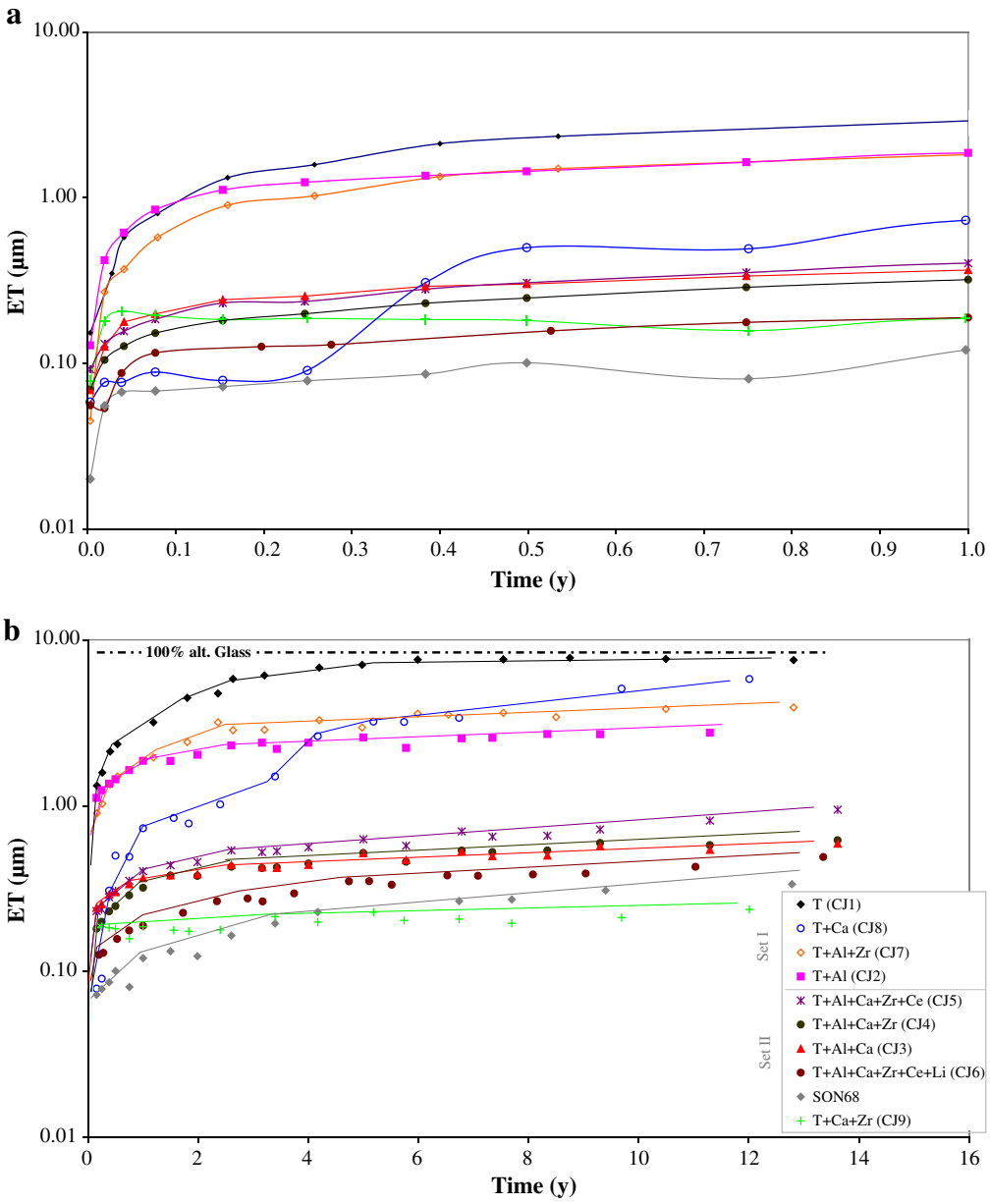

Fig. 1. Altered glass thickness, *ET*(B) as a function of time during the static test at 90 °C. a) from 0 to 1 year. b) up to 14 years.

amounts of other elements, particularly Si. Finally, the effect of Ce is not clear when comparing CJ4 and CJ5. The slight increase in the initial dissolution rate from CJ5 to CJ6 could be due to the increase in the Ce content (Li is expected be to have a negative effect on r_0) but no conclusion can be drawn as the overall compositions of the two glasses are quite different. The value for SON68 is the same as for CJ6, which is logical since CJ6 is the closest in composition to SON68. We will see in the following sections that the behavior of this 8-oxide glass is similar to that of the complex SON68 glass. The present result in dilute conditions suggests either that the elements present in SON68 glass and absent in the CJ6 glass have no significant effect on the initial dissolution rate, or that the other elements have self-compensating effects.

4.1.2. Rate drop and residual alteration rate

The evolution of the equivalent thickness of altered glass, calculated from the boron concentration, is shown in Fig. 1, during the first year (Fig. 1a) and during the whole duration (Fig. 1b).

In static conditions at SA/V of 8000 m^{-1}, the initial dissolution rate is maintained only for a very short time, typically around half an hour [17]. The rates of all glasses drop rapidly by several orders of magnitude and the leaching solutions become more and more concentrated (Fig. 1 and Supporting information). The pH rapidly reaches a steady state around 9, slightly dependant on the glass composition (Table 2) but no significant increase is observed between 1 y and 11 y (Table 2).

Based on the altered glass thicknesses (Fig. 1), two populations of glasses can be distinguished: one contains materials highly altered ($ET(B) > 1$ µm at 11 y) and the other contains glasses significantly less altered ($ET(B) < 1$ µm at 11 y). The first set (set I) of glasses is composed of CJ1, CJ2, CJ7, and CJ8, and the second one (set II) of CJ3 to CJ6, CJ9 and SON68 glasses. The ternary glass CJ1 is fully altered after around 5 y and glass CJ8 is almost fully altered after 11 y. The differences between glasses are more significant here than observed during previous short-term tests in dilute conditions, and can thus be more easily attributed to compositional effects. For example, compared to CJ1, the presence of Al (CJ2) and of Al + Zr (CJ7) decreases the altered glass thickness by factors of 2.5 and 1.5, respectively, after 11 y. CJ8 is less altered than the glasses in set I at the beginning of leaching, but this glass undergoes several resumptions of alteration, leading to

Table 2
Results of the short- and long-term leaching experiments. r_0 is the initial dissolution rate, $r_0/r_{r,1y}$ the rate drop, r_r the residual rate, D the diffusion coefficient of mobile elements through the passivating layer, t_r the time necessary to reach the residual rate. NSH: sodium silicate hydrate; CS: calcium silicate; CSH: calcium silicate hydrate.

Glass	CJ 1	CJ 2	CJ 3	CJ 4	CJ 5	CJ 6	CJ 7	CJ 8	CJ 9	SON68
r_0 ($g \cdot m^{-2} d^{-1}$)	4.5	1.1	2.4	1.7	1.6	2.2	1.1	9.5	8.5	2.2
$pH_{90°C}$ (1 y)	9.3	8.9	9.1	9.0	9.0	9.3	8.7	9.2	9.1	9.2
r (1 y) ($g \cdot m^{-2} d^{-1}$)	1.6E-02	3.2E-03	3.7E-04	4.9E-04	5.4E-04	4.4E-04	3.0E-03	4.7E-03	< 5E-05	4.5E-04
r_0/r_{1y}	280	350	6500	3500	3000	5000	370	2000	>170000	4900
t_r (days)	–	250	250	400	250	250	nd	–	<<100	200
D (m^2/s)	2.6E-19	7.1E-20	1.3E-21	1.4E-21	1.5E-21	3.1E-22	6.9E-20	–	1.0E-23	1.4E-22
$pH_{90\ °C}$ (11 y)	9.1	8.9	9.1	9.0	9.0	9.3	8.7	9.2	9.1	9.3
r_r (11 y) ($g \cdot m^{-2} d^{-1}$)	–	3.8E-04	1.0E-04	1.1E-04	2.2E-04	7.9E-05	4.5E-04	3.3E-03	2.9E-05	1.7E-04
Secondary crystalline phases	Am silica NSH	No	No	No	No	No	No	NSH CS CSH	No	Phyllosilicates

complete alteration before the others (except CJ1). Note that in the case of CJ8 (a linear scale representation is shown in Fig. 10), because the alteration resumes several times the residual rate is not really meaningful. The values given in Table 2 are merely indicative.

Set II includes glasses containing either {Al + Ca} or {Zr + Ca}. These couples of elements lead to significant rate drops and low residual rates. The strong influence of the synergic effect of these elements hides other potential effects when moving from CJ3 to CJ6, as these four glasses behave very similarly. This observation could also be due to the small content of added oxides (ZrO_2, Ce_2O_3, Li_2O). Also note the particular behavior of CJ9 glass, which exhibits a high degree of alteration during the first 14 days of leaching and a very high rate drop followed by a very low residual rate (Fig. 1 and Table 2).

Indeed, these results show that glasses with low initial alteration rates do not have the lowest residual rates: CJ9 has the second highest initial dissolution rate and the lowest residual rate. Conversely, glasses CJ2 and CJ7 have the lowest initial dissolution rates and the highest residual rates (CJ8 is an exception, see below).

The characteristic time, t_r, corresponding to the transition between the rate drop regime and the residual rate regime was estimated from the evolution of the activity of silica for 8 of the 10 studied glasses. For CJ1 and CJ8, it was not possible to estimate this time. Except for CJ4, these durations are close but less than one year, so we can consider that rates calculated after 1 year refer to the beginning of the residual rate regime whereas rates calculated after 11 years give insight into long-term rates. Looking at the results, one can see that the residual rates tend to diminish with time. In fact, the residual rate of CJ2 and CJ7 decreases by factors of 7 and 8 between 1 and 11 years, whereas it diminishes by only a factor of 3 to 4 in the series of glasses CJ3 to CJ6 and SON68. For CJ1 glass, the residual rate was measurable only at 1 year as the glass rapidly reached complete alteration. Finally, the residual rate of CJ9 seems to evolve more slowly than the others, inviting us to pay more attention to this material.

During the residual rate regime (i.e. between 1 and 11 years for most of the glasses), the apparent diffusion coefficients of mobile species through the passivating layer, D, have been derived from leaching data, assuming that diffusion occurred within the whole alteration layer. Fig. 2 shows a good correlation between the estimated effective thickness of the alteration layer, (ET(B)–ET(Si)), and the square root of time, showing that for most of the glasses a single diffusion coefficient satisfactorily describes the release of mobile elements from 1 to 11 years. Table 2 shows that D varies by several orders of magnitude within the series of glasses studied. As expected, CJ1 exhibits the highest value of D. The addition of Al or Zr to this ternary glass diminishes D by a factor of 3, but the most significant decrease is obtained by the addition of Ca to Al (CJ3) or to Zr (CJ9). As for the residual rate, there are no real differences from CJ3 to CJ5, but CJ6 has a lower value of D, quite close to that of SON68 glass. The value obtained on this complex glass is close to the one directly measured by NanoSIMS on a SON68 glass specimen altered for 26 years in a granitic environment [15] and in pure water or silica-doped water by other techniques [20,21]. The lowest value of D by far is obtained with CJ9 glass. However, it was impossible to determine D for CJ8, since there is no linear portion on the curve $e = f(t^{0.5})$. This is due to several resumptions of alteration provoked by the precipitation of silicate minerals.

4.2. SEM characterization of the alteration products

The altered glass powders were characterized by SEM at the end of the experiments.

Fig. 3 shows the main features of the samples, except for CJ5 and CJ7 which are very similar to CJ4 and CJ2, respectively. The SEM observations first confirm that the CJ1 glass is fully altered, the particles have become fleecy and form precipitates more or less agglomerated (Fig. 3a). From CJ2 to CJ7, the grains are covered with a continuous and probably amorphous gel layer, and no secondary crystalline phases are visible (Fig. 3b to e). In case of CJ2, cracks can be seen which no doubt formed during the sample preparation. For thinner gels (CJ3 to CJ6) no cracks are detected. The CJ8 glass is severely altered, most of the alteration products appear as small particles widely distributed in size and more or less crystallized (Fig. 3f). Glass CJ9 exhibits a smooth surface except on areas where a thin external layer of altered glass is detached as shown in the inset (Fig. 3g). The underlying gel appears rough. No secondary crystalline phases were observed on this sample. Conversely, the grains of SON68 glass (Fig. 3h) showed small particles corresponding to phyllosilicate-like minerals, as expected for this type of glass [17,22–24].

4.3. TEM characterization

Ultrathin sections of altered CJ6, CJ7, CJ9 and SON68 glasses were prepared by Focused Ion Beam milling. The pristine glass and the gel composition were analyzed by EDS (Table 3). Note that, due to its

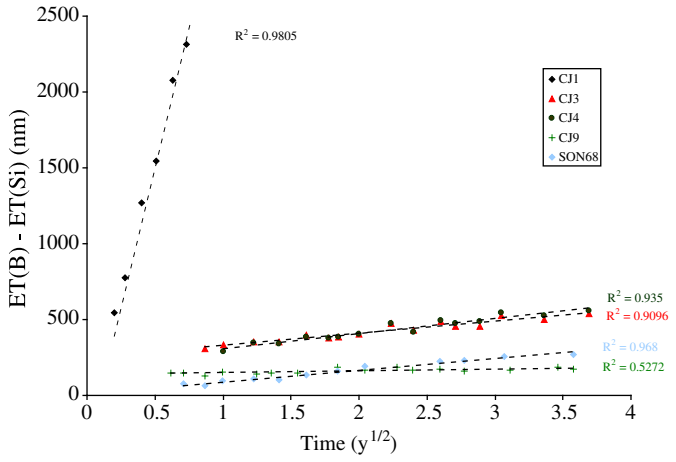

Fig. 2. Thickness of the alteration layer beyond t_r versus the square root of time. The slope of this curve is used to determine the apparent diffusion coefficient of mobile species through the alteration layer.

high mobility, Na is often underestimated (compare the analyzed and expected Na concentrations of the pristine glass). The analyses indicated in Table 3 were carried out on a large area (typically 0.2 μm × 0.2 μm) to minimize this problem. Analyzed and expected concentrations of the other elements are in agreement except for the Zr concentration in CJ6 which is clearly underestimated. Several chemical profiles were obtained along the gel with an electron beam focused at 10 nm (not shown here). All exhibit constant concentrations showing that no chemical gradients occur within the gel (see for example the case of CJ7 gel shown in Fig. 4b). EDS analyses globally show that Si is enriched by 10% to 25% within the gels, compared with the corresponding pristine glass composition; Al is also enriched by around 10%, Zr also with an enrichment of up to 50%, whereas Na is strongly depleted (by a factor of 3 to 7). Ca is also strongly retained within the gels in agreement with the low concentrations measured in solution (see the Supporting information). Except for CJ9, the gel thickness observed by TEM matches the glass alteration thickness calculated from the boron concentration in solution. The bright field image of the gel formed on CJ7 shows no evidence of pores, unlike CJ9 gel which exhibits a well structured porosity (Fig. 4a). At the first order, this difference could be the consequence of the substitution of network-forming Al (in CJ7) for

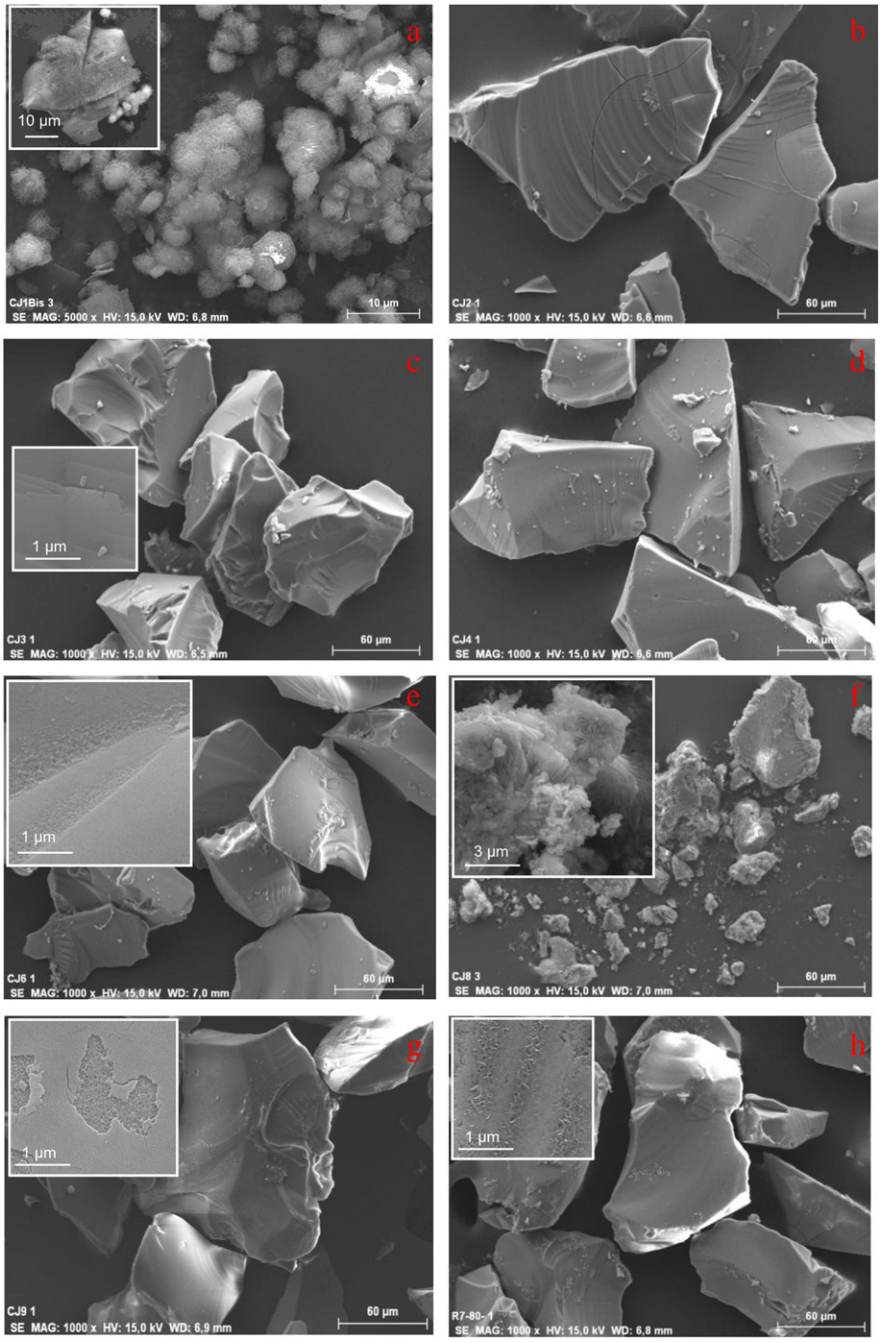

Fig. 3. SEM images of the altered glasses. a) CJ1 glass fully altered and transformed into crystalline phases; b) CJ2 glass forming only a gel, cracked when dried; c) CJ3 glass forming only a gel, thinner than the CJ2 gel, thus uncracked; d) CJ4 glass forming only a gel (some pieces of gel are deposited on the grains); e) CJ6 glass forming only a gel; f) CJ8 glass, almost fully altered and transformed into a gel and calcium silicate minerals; g) CJ9 glass forming a layered gel (external layer partly depleted visible in the inset); h) SON68 glass forming a gel and few crystalline phases (phyllosilicate visible in the inset).

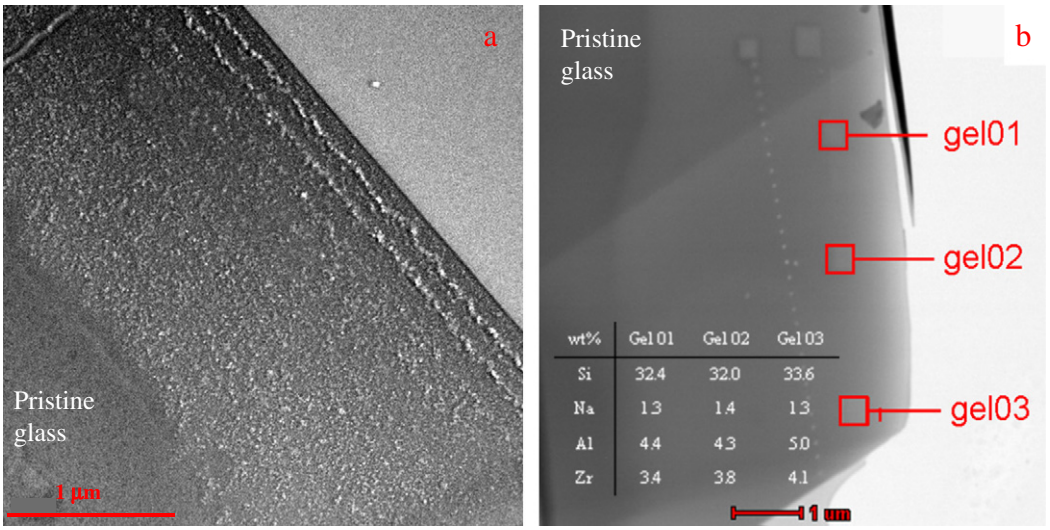

Fig. 4. (a) CJ9 bright field TEM image; (b) CJ7 bright field TEM image and EDS analyses.

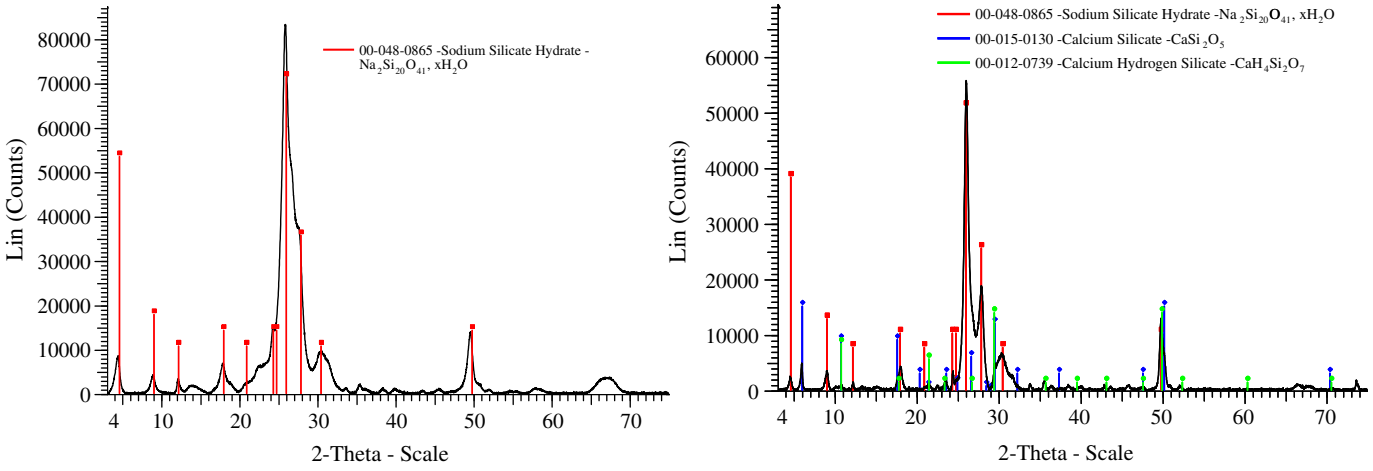

Fig. 5. XRD patterns of altered CJ1 (left) and CJ8 (right).

network-modifying Ca (in CJ9). More generally, such important morphological differences clearly highlight that relatively minor composition changes strongly affect the mechanisms and dissolution rate.

4.4. X-ray diffraction

Characterization by XRD was carried out on altered CJ1 and CJ8 glass powders (Fig. 5), as only these materials showed large amounts of crystalline phases. A sodium silicate hydrate, whose formula is $Na_2Si_{20}O_{41}$, xH_2O, precipitated during CJ1 glass alteration or after its complete alteration. The same phase is observed in the CJ8 glass, as well as calcium silicate hydrates (CSH).

5. Discussion

This section attempts to address several issues raised by the experiments presented in this paper: How does the dissolution rate evolve from short to long term? What are the mechanisms governing short-, medium- and long-term glass alteration? How do elements such as Al, Ca, Zr, Ce affect these mechanisms?

Fig. 6 summarizes the different stages of alteration of nuclear glasses and the corresponding limiting mechanisms. For these borosilicate glasses at neutral and alkaline pH, interdiffusion is rapidly hidden by hydrolysis of the silicate network. This is why both processes are included in the initial rate regime. The rate drop is controlled by affinity effects and diffusion of reactive species through the gel layer which becomes increasingly protective. Beyond the transition time, t_r, the residual rate evolves very slowly, probably

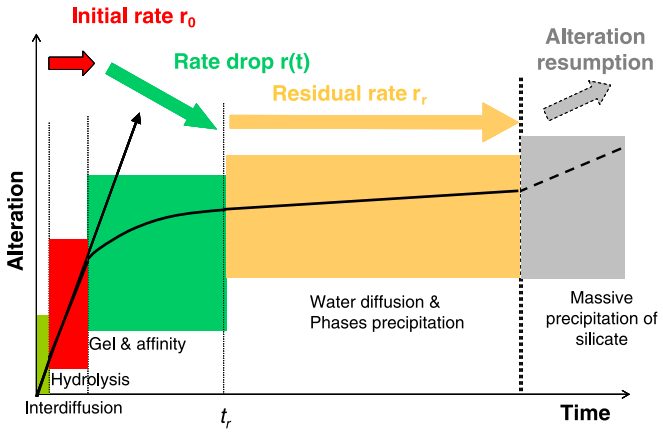

Fig. 6. Stages of nuclear glass alteration and related mechanisms. The duration of each kinetic regime depends on the glass composition and on the leaching conditions (temperature, pH, composition and renewal rate of the solution, etc.).

controlled by water diffusion through the passivating layer (which can be a part of the gel layer) and the precipitation of crystalline phases. In some cases the glass alteration can resume when massive and rapid precipitation of silicate minerals occurs. For more details on this sequence of reactions, refer to recent reviews [17,25]. For practical reasons, we have chosen to organize the discussion according to these four kinetic regimes.

5.1. Initial rate

The first mechanism affecting glass during alteration by water is ion exchange or interdiffusion between the protonated species (H^+, H_3O^+) in solution and network-modifying cations in the glass [26]. In parallel, ionic-covalent bonds of the network-forming elements (Si–O–*X*, where *X* = Si, Al, B, Zr) undergo hydrolysis, resulting in a nucleophilic attack by OH^- [27]. As long as the solution remains sufficiently dilute, the glass dissolution rate remains at a maximum and corresponds to the initial rate (also called the forward rate), noted r_0.

This alteration regime can be qualitatively related to the glass composition and its structure through the distribution of network-forming cations and exchange sites [28]. The values of r_0 in Table 2 show that the addition of Al to the ternary glass (CJ2 vs CJ1) significantly decreases r_0. The structure of CJ2 glass was previously investigated by solid state ^{17}O and ^{27}Al MQMAS NMR showing that Al was distributed in silicate units, forming Si – O – Al bonds (without detectable Al – O – Al bonds). Al is then in tetrahedral units $[AlO_{4/2}]^-$ with Na^+ acting as a charge compensator [29,30]. Thus, the addition of Al in the glass results in a more polymerized network, related to the decrease of modifier cations near nonbridging oxygens (NBO). Under these conditions, the effect of Al on the initial alteration rate may be related both to the decrease of network hydrolysis with the decrease of NBOs [28] and to the low solubility of Al. The distribution of boron species in the aluminosilicate network, through the mixing of [4]Al and [3]B, as well as [3]B(ring)/[3]B(non-ring) ratio, may also influence the dissolution rates; with higher B/Al ratios, boron release was thus correlated with the increase of [3]B(ring), more easily hydrolysable than tetrahedral boron [31].

In the same way, the addition of Zr in the glass has a similar effect (CJ3 vs CJ4 or CJ8 vs CJ9). Zr is inserted in the silicate network forming Si – O – Zr bonds $[ZrO_{6/2}]^-$ mainly compensated by Na cations [32]. The addition of Zr systematically diminishes the initial dissolution rate in borosilicate glass [7]. The high insolubility of Zr results in Si – O – – Zr bonds that are difficult to hydrolyze, strengthening the glass structure and leading to a lower element release and a lower alteration rate. However, this phenomenon is not as strong as with Al (CJ2 vs CJ7). The main possible reason is the lower molar content compared to Al (0.54 mol% Zr in CJ9 vs 1.92 mol% Al in CJ2 for example).

Conversely, in similar dilute media, the addition of Ca to the ternary glass (CJ8 vs CJ1 or CJ3 vs CJ2) results in higher alteration rates, potentially due the decrease in silica content and/or a direct affect associated with the addition of Ca. Such behavior was previously observed in a glass series with increasing Ca content altered at pH 8 [33]. NMR investigations of similar glass compositions showed that Ca mainly acts as a modifier cation near NBOs, rather than as a charge compensator of Al, Zr [30] or B [34]. The addition of Ca thus participates in network depolymerization, and may enhance network hydrolysis. It is worth noting that in the next step of alteration, during the formation of the gel layer, Na is released in solution but the coordination of Al and Zr units remains unchanged due to an exchange of charge-compensating cations leading to compensation by Ca [30,32].

Assuming the effect of a given element on the hydrolysis of the Si – O bond can also be evidenced when supplied from solution, one can consider some literature data. For instance, the unfavorable role of Ca^{2+} in solution on the silica hydrolysis was highlighted by Dove, with the dissolution of quartz in alkali and alkaline-earth chloride solutions [35]. Later, Wallace proposed a mechanism of preferential sites for calcium on the glass surface leading to increased hydrolysis by first principles calculations on $Q^3Si-O_{br}-SiQ^3$ in presence of alkaline earth ions (Mg^{2+}, Ca^{2+}, Ba^{2+}) [36]. Ca weakens the surrounding Si – O interactions by withdrawing electron density from the lone-pair region adjacent to the bridging oxygen. This significantly diminishes the dissociation energy of the Si – O bond, which increases the hydrolysis kinetics. This mechanism is particularly efficient with Ca^{2+}, given the high surface concentration of the complexes formed.

A slight increase in the initial alteration rate is noted between CJ5 and CJ6 when adding Li and Ce. Although the effect of Li can be expected to be equivalent to Na, the role of rare-earth ions on the glass structure and on the initial alteration rate is more involved. Ce is situated in a silicate environment with a coordination number of 8 [37], and probably with Na acting as a charge compensator. However, the small quantities of Ce added here do not appear to impact the alteration rate.

Finally, the glass containing only Si and B as network formers (CJ8) has the highest alteration rate (9.5 $g \cdot m^{-2} d^{-1}$), which is slightly decreased by the addition of Zr (CJ9). This confirms the favorable impact

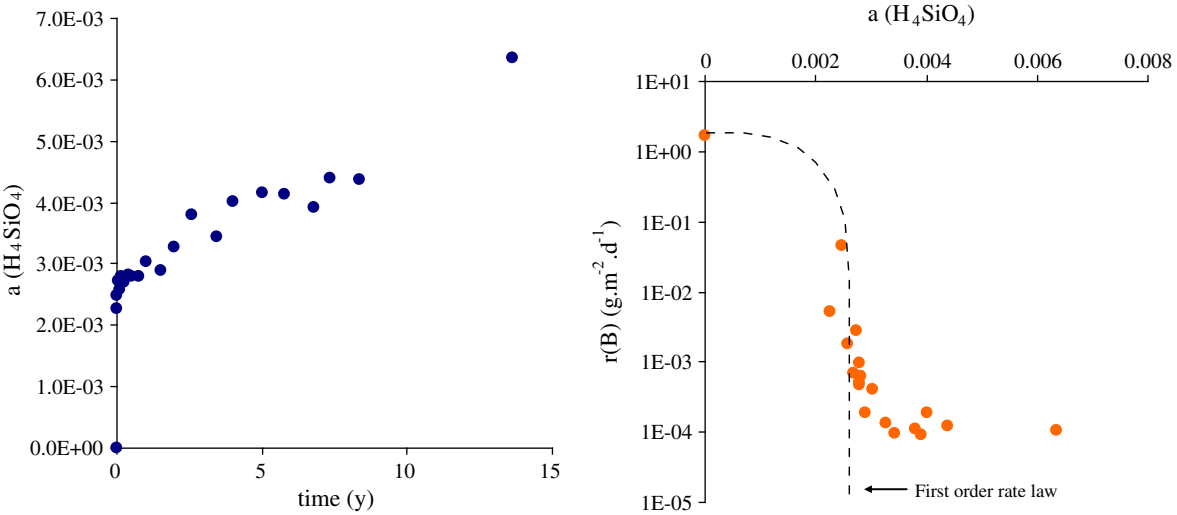

Fig. 7. Activity of orthosilicic acid versus time in the CJ4 experiment (left) and alteration rate of CJ4 versus activity of orthosilicic acid (right).

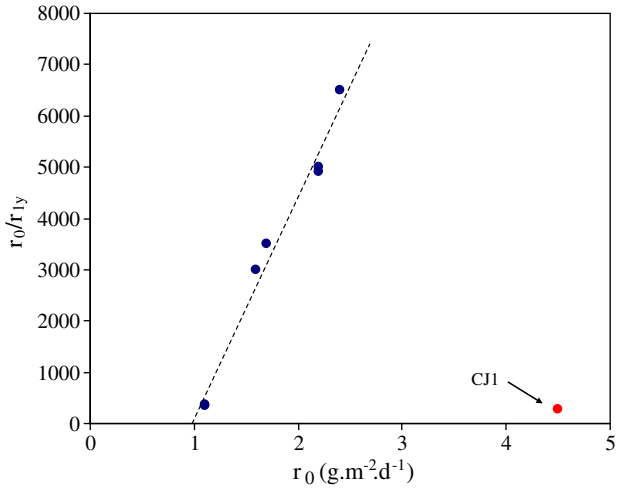

Fig. 8. Rate drop (r_0/r_{1y}) versus initial rate (r_0) in the case of Al-containing glasses and CJ1 glass.

of Al and Zr in strengthening the glass network against hydrolysis reactions and the unfavorable impact on cations acting as network modifiers near nonbridging oxygen atoms (NBOs).

5.2. Rate drop

In a confined medium such as the static tests run at high SA/V, the initial rate is not the dominant regime after a few hours. For all the tested glasses, the dissolution rate rapidly drops by several orders of magnitude. However it is interesting to note that this drop occurs more or less rapidly and with different intensity depending on the glass composition. Two coupled processes are assumed to control the rate drop: one based on thermodynamics, the other on transport [17,25,38]. Indeed, the increase in the silica concentration near the hydrated glass can be expected to decrease the affinity of the reaction of hydrolysis of the Si – O bonds. The first kinetic model inspired by Transition State theory established a simple relation between the glass dissolution rate and the activity of silica at the glass surface [39]:

$$r = r_0\left(1-\frac{a_{H_4SiO_4}}{a^*_{H_4SiO_4}}\right) \quad (9)$$

where r_0 is the initial dissolution rate and a^*_{H4SiO4} is the activity of silica at equilibrium. This law was called the *first-order law*.

Further theoretical [40] and experimental work [41] showed that this model was insufficient to properly describe the glass dissolution mechanisms. Evidence of a diffusion-limiting step was shown experimentally using various approaches [15,21,42–45]. Now, kinetic models applied to glass dissolution couple the affinity and protective properties of the alteration layer [17,48].

We performed speciation calculations with JChess software [13] on our leaching data and found an unexpected result. As shown in Fig. 7, the activity of silica increases slowly but never reaches a plateau as should have occurred in case of equilibrium between the hydrated glass and solution. The first-order law fits only the first few data points but deviates considerably when the rate reaches a near-constant value. This result, presented here for CJ4 glass, can be generalized to the other glasses. The possible reasons for such behavior are discussed in the next section. Because no objective criterion for defining the transition between the rate drop regime and the residual rate regime was available until now, we suggest using the turning point of the $r = f(a(H_4SiO_4))$ curve to estimate the beginning of the residual rate regime. The corresponding characteristic time, t_r, is reported in Table 2. We may note that this time, when calculable, is around one year except for CJ9 glass ($t_r \ll 100$ d) which exhibits specific behavior. This could be due to the fact that the SA/V ratio for the CJ9 test was twice that of the other tests: it can be expected that the higher SA/V, the shorter duration of the rate drop regime. Despite this specific case, we can consider that the rates calculated at 1 year correspond to the beginning of the residual rate regime.

Note that the calculation of the silica activity in the leachates does not take into account all the potential species present. According to recent papers [46,47], tens of oligomers and nanocolloids can be found depending on the temperature, pH, ionic strength, and concentrations of other ions. For this reason, it should be interesting to reconsider these results once a full characterization of the silica species within our leachates becomes available.

This study provided a paradoxical result recently discussed in the literature. As illustrated in Fig. 8 for glasses containing Al, those dissolving faster initially exhibit the highest rate drops and the lowest residual rates. Indeed, as explained by Cailleteau and coworkers, this behavior is a consequence of the gel restructuring [33]. A high r_0 implies a high rate of silica hydrolysis. As silica undergoes reactions of depolymerization and repolymerization (hydrolysis and condensation), especially in the pH range of our experiments [27], if a high

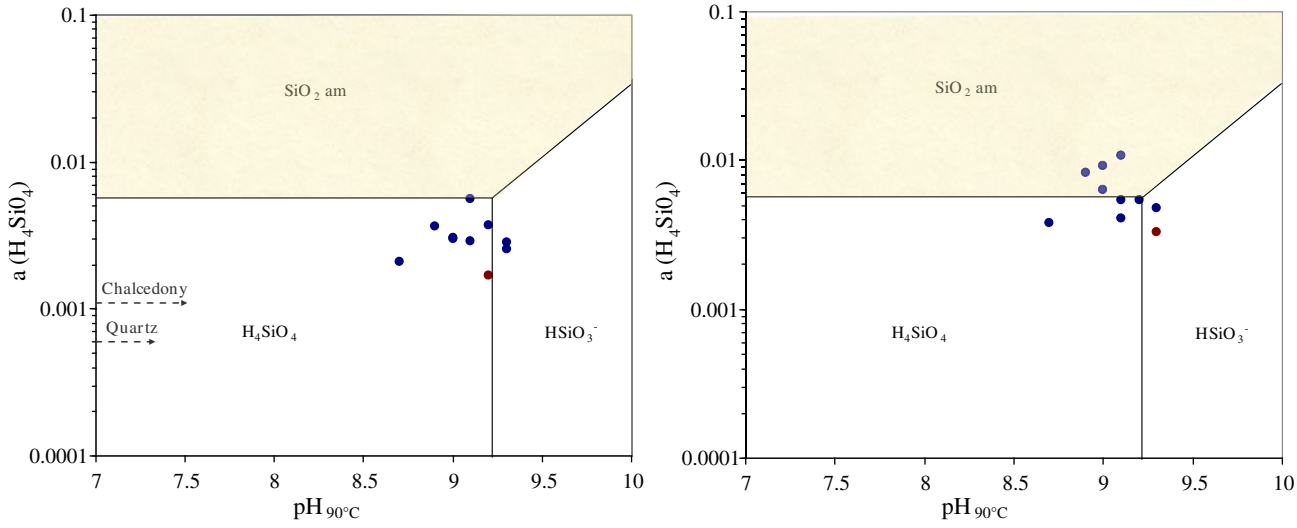

Fig. 9. Speciation diagram showing the activity of silica for the ten glasses after 1 y (left) and at the end of the experiment (between 12.8 y and 14.4 y depending on the glass). The brown dot corresponds to SON68 glass.

concentration of silica is reached quickly, the polymerization of the gel network is accelerated. Moreover, to minimize its free energy, the gel favors the coalescence and elimination of the pores, and replaces poorly bound species by connected species [7,47,49,50]. In other words, the effectiveness of the gel can be measured by its restructuring capacity, at short range (Q_n species) and medium range (porosity). Unfortunately, reality is more complex and the gel reorganization does not depend only on silica behavior. A high level of silica condensation and/or a thick gel does not necessarily mean a highly protective gel layer. As an example, the CJ1 gel formed by coalescence of amorphous silica spherules [5] is not very protective compared with the Al-rich material (Fig. 6) even thicker and fully polymerized (only Q_4 species). Conversely, CJ9 shows that with a thin gel (about 200 nm) having the right proportions of Si, Zr and Ca, protectiveness is ensured and the residual alteration rate is 1000 times lower.

5.3. Residual rate

In this section we first attempt to determine the mechanisms underlying the residual rate, as this subject is still open to debate, and then discuss the effects of glass composition on this regime. In the current but likely incomplete state of our understanding, the residual rate could be controlled by a set of potentially coupled processes: ion exchange, water diffusion through the passivating layer, transformation of the passivating layer into a porous gel layer, and precipitation of crystalline phases [15,17,51]. Can the experiments performed in this study provide a better understanding of the key mechanisms controlling the residual rate? What might be the long-term evolution of the residual rate, as no thermodynamic equilibrium between the glass and the solution will ever be achieved?

For most of the glasses of this work (all except CJ1, CJ7 and CJ8), the residual rate regime runs from one year up to the last data point. CJ1 and CJ7 glasses do not show the turning point allowing the calculation of the transition time t_r between the rate drop and residual rate regimes. Moreover, due to the numerous resumptions of alteration undergone by CJ8 glass, it is not possible to contemplate a residual regime for this material.

Here we show a slow but significant decrease in the residual rate over time (Table 2). Except for CJ1, which was fully altered after only a few years, rates measured at 11 years are systematically lower by a factor of 3 to 9 than the rates obtained after just one year of leaching. Even the residual rate of SON68 glass, on which phyllosilicates precipitate, decreases, whereas previous papers were not conclusive due to experimental uncertainties [2,3]. However, the residual rate of this glass calculated at 11 years ($1.7\times10^{-4}\,g\cdot m^{-2}d^{-1)}$ is very close to values from other experiments conducted at lower or higher SA/V ratios [2,3,52]. Moreover, in our study, it is not possible to measure a significant difference between rates measured after an intermediate duration, like 5 years, and after 11 years. Thus even a test lasting 11 years does not allow us to conclude about the long-term evolution of the residual rate from direct rate measurements. This necessarily requires a mechanistic approach and a model relating the mechanisms and rate.

We did not see any marked dependence between the residual rate of the studied glasses and the activity of silica in solution. Fig. 9 shows the general trend: during the residual rate regime the activity of silica slowly increases to saturation with respect to amorphous silica, whereas the residual rate of most of the glasses decreased very slowly. For 6 of the studied glasses, saturation with respect to amorphous silica occurs before the last sampling interval; for the other glasses, including complex SON68 glass, the solution remains slightly undersaturated, even though it has significantly evolved since the first year of leaching. The future evolution of CJ6 and SON68 glasses will chiefly depend on the evolution of the pH, which is very near the pKa of the $H_4SiO_4 \leftrightarrow H_3SiO_4^- + H^+$ reaction. If silica affects the residual rate, this must be very different from what was observed during the rate drop regime. Recently, Neeway and coworkers obtained a decrease in the water diffusion coefficient within the SON68 glass by adding silica to the leaching solution [52]. This interesting finding indicates that diffusion processes take place through a layer that has reacted with the interfacial fluid. This is consistent with data obtained on a SON68 glass sample leached for 26 years in a granitic environment [15]. The passivating zone of this material, which incorporated exogenous element supplied by the solution, was located in the internal part of the hydrated glass. According to McGrail, the deviation from a pure affinity concept as illustrated in Fig. 7 could be explained by the pursuit of ion exchange processes [51]. The authors claimed that this phenomenon is the main contributor to the residual rate of boron-free aluminosilicate glasses. Note that a pH rise resulting from this phenomenon is not observed in our study (Table 2), because of the buffering capacity of boron released during glass leaching. Note also that, focusing on the consequences of the leaching processes, we are not able to discriminate between ion exchange and diffusion of mobile elements through the passivating layer. This would require the use of dedicated, sensitive and accurate probes. Recently, we have suggested that the irreversible reaction of in situ transformation of the hydrated glass resulting from ion exchange process into a porous gel could also be a key reaction occurring during the residual stage [15]. Here we see that, based on morphological aspects, the alteration layer of CJ9 glass looks like a porous gel whereas the alteration layers of CJ6 and CJ7 more closely resemble hydrated glass. Such differences are surprising and remain unexplained. Further investigations are required in order to elucidate this issue. One promising route is to investigate how water dynamic and reactivity is affected by pore size and by the chemistry of the walls [53].

Our results also confirm that massive precipitation of secondary crystalline phases does affect the residual rate. Calcium silicate and sodium silicate certainly sustain CJ8 glass dissolution, impeding the formation of an effective diffusive barrier and consequently leading to a sudden resumption of alteration (see Section 5.4). In the case of SON68 glass, precipitation of small amount of phyllosilicate is not sufficient to impede diffusive behavior during the residual rate regime (Fig. 2). One can imagine that if the glass had contained large amounts of elements favoring the precipitation of phyllosilicates such as Mg, Zn, Ni, and Co, the rate would have been higher and more linear [2,54].

To summarize the contribution of this study to an overall understanding of the mechanisms controlling the residual rate, we can conclude that diffusion of water and mobile species of the glass through a reactive and protective layer is probably a key phenomenon controlling this regime as well as precipitation of silicate minerals. The role of the macroporous gel, when it forms remains unclear and requires further investigation. For example, we do not know whether the slow evolution of the silica activity is related to the gel aging. Moreover, a slight variation in the glass composition strongly affects the mechanisms and the residual rate. Let us now address this issue.

We did not see any correlation between the residual rate and the glass composition (fraction of mobile elements, fraction of silica or silica plus alumina, etc.). However there are some interesting findings resulting from this series of experiments. First, the addition of Al to the ternary glass (CJ2 vs CJ1) or the addition of Al + Zr to the ternary glass (CJ7 vs CJ1) significantly decreases the residual rate but this effect requires a long time. In comparison, the rate drops by three orders of magnitude more quickly in some other glasses. This is due to the structural role of Al and Zr. They are considered in many papers as glass and gel hardeners [47,49,55]. This means that because Al – O and Zr – O have a higher bond energy than Si – O, the Si atoms near the hardeners are not easily hydrolyzed and thus cannot participate in the gel restructuring. It is known that the gel progressively reorganizes by steps of hydrolysis and condensation to minimize its energy, and that the steric obstruction created by the insoluble Zr clusters disturbs this process, which results in greater porosity and specific surface area of the gel, and thus in higher diffusivity. Here, because the amount of Al and Zr is not too high, the consequences are a decrease in the initial rate and higher diffusivity and a longer time to reach

very low rates (Table 2). We can imagine that if the amount of Al or Zr had been sufficiently high to impede the gel restructuring, and in the absence of secondary crystalline phases, the initial rate would have been very low but would not have decreased with time, or very slowly. That is what is expected from Cailleteau's work [33,45].

The addition of Ca to the ternary glass (CJ8) dramatically affects the rate drop, especially during the first hundred days (Fig. 10), but this effect is quickly cancelled by the precipitation of CSH like minerals. The addition of Ca to the "ternary + hardener element" systems (CJ3 vs CJ2 or CJ9 vs CJ7), dramatically reduces the residual rate. This is very spectacular in the case of CJ9, for which the residual rate at 11 years is 13 times lower than for CJ2. In the pH range of our experiment, Ca is fully retained within the gel layer (Table 4) and should play a major role in the gel restructuring process. In the case of CJ9 it has been shown that Ca^{2+} preferentially compensates the charge of $[ZrO_{6/2}]^{2-}$ units [56], which increases alkali solubility ($RF(Na) = 0$). In previous work at high Ca and Zr content (~9%), it led to the formation of 10 Å pores in the gel [56], of the same order of magnitude as the diffusing hydrated ions. Moreover, another diffusion barrier is added by the gel densification observed at the gel/solution interface by TEM. This is consistent with the results obtained by Cailleteau on a very similar glass by ^{29}Si tracing coupled with ToF-SIMS [57]. It corresponds to superficial pore clogging, enhanced by the strong hydrolysis at the beginning of leaching.

In the case of Al-containing glasses (CJ3 to CJ6 and SON68), ab initio calculations would explain the affinity of Al for Ca by the energy stability of Al – O – Al – O – Si – O – Si chains [58]. It is shown that Ca compensates the charge of the two following Al atoms. Moreover, Ca is able to condense by olation [59], contrary to alkalis which remain isolated within the gel structure or simply as aqueous species. Ca leads to a high degree of reticulation with the heavy elements, which likely decreases the pore size, and thus the diffusion of the soluble elements through the passivation layer. Chave recently studied the leaching of CJ7 in Ca solutions [11]. The alteration layer were shown to incorporate Ca from solution, which results in much lower long-term alteration rates. These results are fully consistent with this study and confirm the importance of condensation of Ca and insoluble elements in the gel for ensuring the durability of the glass.

The role of rare-earth elements (REE) remains not clear. Comparing CJ5 with CJ4 we do not see any significant variation of the residual rate whereas the comparison between CJ5 and CJ6 indicates a slight decrease in the residual rate when adding more Ce, although CJ6 contains propositionally more alkali than CJ5 and the resulting pH is slightly higher. The effect of Ce cannot be deconvoluted from the other effects. In our glasses Ce appears to be incorporated homogeneously within the gel whereas the REE are shared between apatite minerals (due to the presence of phosphorus) and the gel in the case of SON68 [60].

Finally, we may note that despite its simple composition, CJ6 glass alteration over 11 years was very similar to that of SON68 glass, with the same initial alteration rate and very close residual rates. We can thus conclude that CJ6 is the best analog of SON68 glass, and can account for its main alteration mechanisms despite the absence of secondary crystalline phases.

5.4. Resumption of alteration

The case of CJ8 is particular: the system never reaches the normal residual regime, and alteration is observed to resume repeatedly until the glass is altered to the core.

Therefore the absence of insoluble elements in the "ternary + Ca" system does not ensure the same protectiveness, or only for a short period of time (around 90 days). Ca is retained in the gel layer, but also in calcium silicate hydrates. Geochemical calculation with JChess indicates that the solution of CJ8 at 90 days is slightly undersaturated with respect to okenite, a calcium silicate hydrate available in the CTDP database and close to the phase detected by XRD (saturation index ($\log Q/K$) of −0.38) and at equilibrium with kenyaite, a sodium

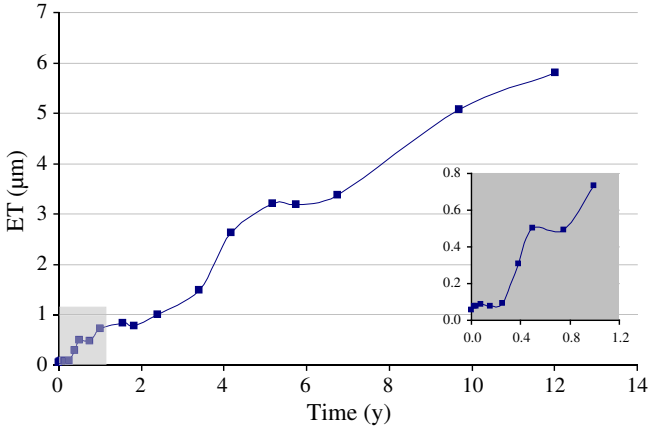

Fig. 10. Evolution of the glass alteration thickness of CJ8 glass during the static test at 90 °C.

silicate hydrate available in the CTDP database and close to the phase detected by XRD (saturation index of −0.17). Then one can think that the first alteration resumption is due to the precipitation of kenyaite and that the calcium silicate mineral precipitates later. As a result, these phases grow by depleting the gel of its structuring elements (Si and Ca), likely increasing the porosity and allowing aqueous species to percolate rapidly through the gel. Alteration thus resumes repeatedly until complete leaching of the glass. Note that a clear interpretation of the underlying mechanisms is difficult as most of the glass grains are fully altered when sampled for characterization. A new experiment should be run and the solid should be sampled at regular intervals to follow the gel evolution when disturbed by the growth of secondary minerals. In general, it is acknowledged that the study of such crystalline phases is of primary importance for predicting glass alteration over the long term, since they can destabilize the gel and significantly decrease its protective properties. Zeolites are known to be responsible for the resumption of alteration of nuclear glasses [61], especially at pH above 10.5 [62]. We attempted to detect such phases in the Al-containing glasses of the series, but neither microscopy nor solution analyses (pH or decreasing Al content) indicated their precipitation. However, the geochemical calculation performed with JChess gave a saturation index for analcime ($NaAlSi_2O_6 \cdot H_2O$) of about 2 after one year and about 2.8 after 11 years. Given the pH of the experiments (around 9), this is consistent with the previous results showing no zeolites at 90 °C below pH 10.5 but remains difficult to interpret as thermodynamics allow their precipitation. Moreover, it is known that zeolites precipitate as the ultimate stage of palagonitization of basaltic glass [63]. We may wonder why such phases did not precipitate in our experiments. One reason could be that nucleation did not occur as supersaturation was not sufficient. Thus, it would have to be activated by a higher pH and with higher concentrations in solution. In this case, it is just a question of time. Another reason could be that nucleation did occur, but with a very small amount of Al in solution. Indeed, at pH around 9, the Al concentration remains low compare to values observed at pH around 11 [63]. Nucleation would thus immediately consume the available Al, which can no longer enable crystal growth. In that case, zeolite will never precipitate in this experiment and the residual rate will certainly continue to decrease slowly.

6. Conclusion

This study has shown that the choice of simplified glasses is relevant to account for the alteration mechanisms involved in more complex systems, such as the R7T7-type glass. In that sense it has been shown that the CJ4 glass, selected by the international community

Table 3
Pristine glass and gel compositions analyzed by TEM–EDS in CJ6, CJ7, CJ9 and SON68. Data correspond to mean values obtained from 3 analyses. Standard deviation is around 10%.

Glass	CJ6			CJ7			CJ9			SON68		
Content (wt%)	Pristine glass expected	Pristine glass TEM	Gel	Pristine glass expected	Pristine glass TEM	Gel	Pristine glass expected	Pristine glass TEM	Gel	Pristine glass expected	Pristine glass TEM	Gel
Si	24.6	27.6	30.5	27.6	28.6	32.0	28.0	28.9	35.6	21.1	22.6	28.2
Na	7.65	6.0	1.8	9.7	4.9	1.4	9.6	3.7	0.5	7.5	7.4	2.4
Ca	3.33	2.8	3.4	–	–	–	3.8	3.2	3.8	2.9	3.1	3.9
Al	3.01	3.1	3.6	3.4	3.9	4.3	–	–	–	2.6	2.9	3.4
Ce	3.9	4.3	4.3	–	–	–	–	–	–	0.8	1.2	0.6
Zr	2.27	1.0	2.7	2.5	2.5	3.8	2.6	2.5	3.7	2.0	2.3	2.8

Table 4
Retention factors, $RF(i)$ calculated after 11 years from the solution analyses. Nc: not calculated (Al was not analyzed in the corresponding experiment).

Glass	CJ1	CJ2	CJ3	CJ4	CJ5	CJ6	CJ7	CJ8	CJ9	SON68
RF(Si)	0.99	0.98	0.91	0.91	0.91	0.84	0.99	0.98	0.80	0.80
RF(Al)	–	Nc	0.99	0.99	1.00	1.00	1.00	–	–	0.97
RF(Na)	0.35	0.42	0.13	0.20	0.19	0.32	0.55	0.21	−0.03	0.20
RF(Ca)	–	–	1.00	0.98	0.98	0.99	–	1.00	1.00	1.00
RF(Li)	–	–	–	–	–	-0.10	–	–	–	0.10

as a reference for improving the knowledge on glass alteration phenomena, can be considered as a good analog of actual nuclear glasses. This is also the case of the more complicated CJ5 and CJ6 glasses. Moreover the long-term experiments discussed in this paper provide new insight into how elements such as Al, Ca and Zr affect the residual rate of borosilicate glasses. Lessons can be drawn from this study: some effects are remarkable (synergy between Al and Ca or Zr and Ca). The residual rates remain difficult to predict as the chemical reactions and transport phenomena are coupled at nanoscale. Moreover our findings could likely be modified by changing the leaching conditions (temperature, pH, solution composition, glass composition, etc.), as it is known for example that the relative solubility of the concerned elements strongly depends on the pH. It is thus of primary importance to better understand the role of the key elements within nuclear glass on the gel properties and the competition between the gel and the crystalline phases capable of precipitating.

Acknowledgments

The authors are grateful to the two anonymous referees whose remarks and insights contributed to significant improvements of the manuscript. We also thank Martiane Cabié from Aix-Marseille University (CP2M) for the preparation of the FIB cross sections and the TEM characterization.

Appendix A. Supplementary data

Supplementary data to this article can be found online at http://dx.doi.org/10.1016/j.jnoncrysol.2012.05.024.

References

[1] C. Poinssot, S. Gin, J. Nucl. Mater. 420 (2012) 182.
[2] E. Curti, J.L. Crovisier, A.M. Karpoff, G. Morvan, Appl. Geochem. 21 (2006) 1152.
[3] P. Frugier, S. Gin, J.E. Lartigue, E. Deloule, Mater. Res. Soc. Symp. Proc. 392 (2006) 305.
[4] L. Trotignon, J.C. Petit, G. Dellamea, J.C. Dran, J. Nucl. Matter. 190 (1992) 228.
[5] C. Jegou, S. Gin, F. Larche, J. Nucl. Mater. 280 (2000) 216.
[6] A. Ledieu, F. Devreux, P. Barboux, L. Sicard, O. Spalla, J. Non-Cryst. Solids 343 (2004) 3.
[7] C. Cailleteau, C. Weigel, A. Ledieu, P. Barboux, F. Devreux, J. Non-Cryst. Solids 354 (2008) 117.
[8] F. Pacaud, N. Jacquet-Francillon, A. Terki, C. Fillet, Mater. Res. Soc. Symp. Proc. 127 (1988) 105.
[9] C. Jegou, PhD thesis, Université de Montpellier II, France, 1998.
[10] S. Gin, P. Frugier, Mater. Res. Soc. Symp. Proc. 757 (2003) 175.
[11] T. Chave, P. Frugier, S. Gin, A. Ayral, Geochim. Cosmochim. Acta 75 (2011) 4125.
[12] B.E. Scheetz, W.P. Freeborn, D.K. Smith, C. Anderson, M. Zolensky, W.B. White, Mater. Res. Soc. Symp. Proc. 44 (1985) 129.
[13] J. van der Lee, L. De Windt, V. Lagneau, Comput. Geosci. 29 (2003) 265.
[14] CTDP, Common Thermodynamic Database Project, http://ctdp.ensmp.fr/.
[15] S. Gin, C. Guittonneau, N. Godon, D. Neff, D. Rebiscoul, M. Cabie, S. Mostefaoui, J. Phys. Chem. C 115 (2011) 18696.
[16] T. Chave, P. Frugier, A. Ayral, S. Gin, J. Nucl. Mater. 362 (2007) 466.
[17] P. Frugier, S. Gin, Y. Minet, T. Chave, B. Bonin, N. Godon, J.E. Lartigue, P. Jollivet, A. Ayral, L. De Windt, G. Santarini, J. Nucl. Mater. 380 (2008) 8.
[18] M.I. Ojovan, A. Pankov, W.E. Lee, J. Nucl. Mater. 358 (2006) 57.
[19] K. Benzerara, N. Menguy, N.R. Banerjee, T. Tyliszczak, G.E. Brown, F. Guyot, Earth Planet. Sci. Lett. 260 (2007) 187.
[20] D. Rebiscoul, F. Rieutord, F. Ne, P. Frugier, R. Cubitt, S. Gin, J. Non-Cryst. Solids 353 (2007) 2221.
[21] K. Ferrand, A. Abdelouas, B. Grambow, J. Nucl. Mater. 355 (2006) 54.
[22] J. Caurel, E.Y. Vernaz, D. Beaufort, Mater. Res. Soc. Symp. Proc. (1990) 309.
[23] J.L. Crovisier, E. Vernaz, J.L. Dussossoy, J. Caurel, Appl. Clay Sci. 7 (1992) 47.
[24] E. Vernaz, S. Gin, C. Jegou, I. Ribet, J. Nucl. Mater. 298 (2001) 27.
[25] P. Van Iseghem, M. Aertsens, S. Gin, D. Deneele, B. Grambow, D. Strachan, P. McGrail, G. Wicks, Ceram. Trans. 207 (2009) 115.
[26] R.H. Doremus, J. Non-Cryst. Solids 19 (1975) 137.
[27] B.C. Bunker, D.R. Tallant, T.J. Headley, G.L. Turner, R.J. Kirkpatrick, Phys. Chem. Glasses 29 (1988) 106.
[28] B.C. Bunker, J. Non-Cryst. Solids 179 (1994) 300.
[29] F. Angeli, T. Charpentier, S. Gin, J.C. Petit, Chem. Phys. Lett. 341 (2001) 23.
[30] F. Angeli, M. Gaillard, P. Jollivet, T. Charpentier, Geochim. Cosmochim. Acta 70 (2006) 2577.
[31] E.M. Pierce, L.R. Reed, W.J. Shaw, B.P. McGrail, J.P. Icenhower, C.F. Windisch, E.A. Cordova, J. Broady, Geochim. Cosmochim. Acta 74 (2010) 2634.
[32] F. Angeli, T. Charpentier, M. Gaillard, P. Jollivet, J. Non-Cryst. Sol. 354 (2008) 3713.
[33] C. Cailleteau, F. Devreux, O. Spalla, F. Angeli, S. Gin, J. Phys. Chem. C 115 (2011) 5846.
[34] F. Angeli, T. Charpentier, D. de Ligny, C. Cailleteau, J. Amer. Ceram. Soc. 93 (2010) 2693.
[35] P.M. Dove, C.J. Nix, Geochim. Cosmochim. Acta 61 (1997) 3329.
[36] A.F. Wallace, G.V. Gibbs, P.M. Dove, J. Phys. Chem. A 114 (2010) 2534.
[37] P. Jollivet, C. Lopez, C. Den Auwer, E. Simoni, J. Nucl. Mater. 346 (2005) 253.
[38] D. Rebiscoul, A. Van der Lee, F. Rieutord, F. Né, O. Spalla, A. El-Mansouri, P. Frugier, A. Ayral, S. Gin, J. Nucl. Mater. 326 (2004) 9.
[39] B. Grambow, Mater. Res. Soc. Symp. Proc. 12 (1985) 15.
[40] S. Gin, C. Jegou, P. Frugier, Y. Minet, Chem. Geol. 255 (2008) 14.
[41] Y. Linard, T. Advocat, C. Jegou, P. Richet, J. Non-Cryst. Solids 289 (2001) 135.
[42] S. Gin, Mater. Res. Soc. Symp. Proc. 663 (2001) 207.
[43] S. Gin, I. Ribet, M. Couillard, J. Nucl. Mater. 298 (2001) 1.
[44] D. Rebiscoul, P. Frugier, S. Gin, A. Ayral, J. Nucl. Mater. 342 (2005) 26.
[45] C. Cailleteau, F. Angeli, F. Devreux, S. Gin, J. Jestin, P. Jollivet, O. Spalla, Nat. Mater. 7 (2008) 978.
[46] G.A. Icopini, S.L. Brantley, P.J. Heaney, Geochim. Cosmochim. Acta 69 (2005) 293.
[47] C.T.G. Knight, R.J. Balec, S.D. Kinrade, Angew. Chem. Int. Ed. 46 (2007) 8148.
[48] B. Grambow, R. Muller, J. Nucl. Mater. 298 (2001) 112.
[49] A. Ledieu, F. Devreux, P. Barboux, Phys. Chem. Glasses 46 (2005) 12.
[50] F. Devreux, A. Ledieu, P. Barboux, Y. Minet, J. Non-Cryst. Solids 343 (2004) 13.
[51] B.P. McGrail, J.P. Icenhover, D.K. Shuh, P. Liu, J.C. Darab, D.R. Baer, S. Thevuthasen, V. Shutthanandan, M.H. Engelhard, C.H. Booth, P. Nachimuthu, J. Non-Cryst. Solids 296 (2001) 10.
[52] J. Neeway, A. Abdelouas, B. Grambow, S. Schumacher, J. Nucl. Mater. 415 (2011) 31.
[53] I. Matar Briman, D. Rebiscoul, O. Diat, J.M. Zanotti, P. Jollivet, P. Barboux, S. Gin, J. Phys. Chem. C 116 (2012) 7021.
[54] B. Thien, N. Godon, A. Ayral, S. Gin, J. Nucl. Mater. 427 (2012) 297.
[55] M. Lobanova, A. Ledieu, P. Barboux, F. Devreux, O. Spalla, J. Lambard, Mater. Res. Soc. Symp. Proc. 713 (2002) 571.
[56] O. Deruelle, P. Barboux, O. Spalla, S. Ricol, J. Lambard, E. Vernaz, 5th European Ceramic Conference. Euro Ceramics V. Versailles, France, 132, 2001, p. 2240.
[57] P. Jollivet, F. Angeli, C. Cailleteau, F. Devreux, P. Frugier, S. Gin, J. Non-Cryst. Solids 354 (2008) 4952.
[58] J.A. Tossell, G. Saghi-Szabo, Geochim. Cosmochim. Acta 61 (1997) 1171.
[59] J.P. Jolivet, M. Henry, J. Livage, J. *De la solution à l'oxyde*, EDP Sciences Ed, 1994.
[60] S. Gin, C. Jégou, E. Vernaz, Appl. Geochem. 15 (2000) 1505.
[61] D.M. Strachan, T.L. Croak, J. Non-Cryst. Solids 272 (2000) 22.
[62] S. Ribet, S. Gin, J. Nucl. Mater. 324 (2004) 152.
[63] J.L. Crovisier, T. Advocat, J.L. Dussossoy, J. Nucl. Mater. 321 (2003) 91.